pubs.acs.org/Biomac

Article

Mussel-Inspired Multiloop Polyethers for Antifouling Surfaces

Suebin Park, Minseong Kim, Jinwoo Park, Woojin Choi, Jinkee Hong, Dong Woog Lee,* and Byeong-Su Kim*

Cite This: *Biomacromolecules* 2021, 22, 5173−5184

Read Online

ACCESS | Metrics & More | Article Recommendations | Supporting Information

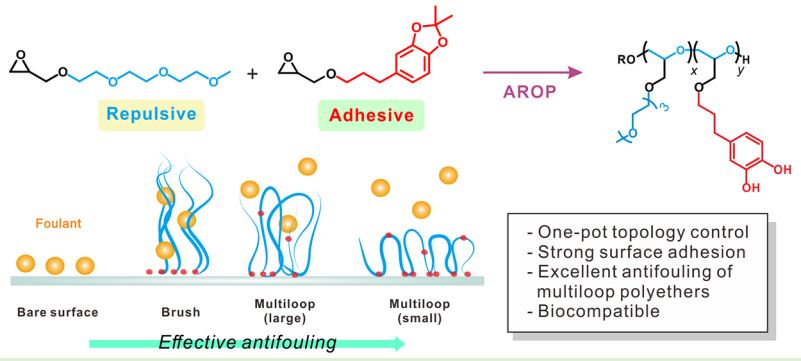

ABSTRACT: Despite the widespread use of polymers for antifouling coatings, the effect of the polymeric topology on the antifouling property has been largely underexplored. Unlike conventional brush polymers, a loop conformation often leads to strong steric stabilization of surfaces and antifouling and lubricating behavior owing to the large excluded volume and reduced chain ends. Herein, we present highly antifouling multiloop polyethers functionalized with a mussel-inspired catechol moiety with varying loop dimensions. Specifically, a series of polyethers with varying catechol contents were synthesized via anionic ring-opening polymerization by using triethylene glycol glycidyl ether (TEG) and catechol-acetonide glycidyl ether (CAG) to afford poly(TEG-*co*-CAG)$_n$. The versatile adsorption and antifouling effects of multiloop polyethers were evaluated using atomic force microscopy and a quartz crystal microbalance with dissipation. Furthermore, the crucial role of the loop dimension in the antifouling properties was analyzed via a surface force apparatus and a cell attachment assay. This study provides a new platform for the development of versatile antifouling polymers with varying topologies.

INTRODUCTION

Biofouling refers to a phenomenon in which various undesired proteins and microorganisms are deposited on surfaces or devices. Notably, it reduces the performance and/or increases the operating costs of devices and equipment, including bioseparation, industrial, and marine equipment, and can even lead to catastrophic incidents such as contamination of medical devices and implants.[1,2] Therefore, realizing a surface with antifouling properties has become imperative to avoid the aforementioned issues.

In this context, over the past few decades, hydrophilic polymers with low polymer−water interfacial energy have been proposed for use as antifouling materials; representative examples include poly(ethylene glycol) (PEG),[3−6] poly(alkyl-2-oxazoline),[7−9] poly(vinyl pyrrolidone),[10−12] and zwitterionic poly(2-methacryloyloxyethyl phosphorylcholine).[13,14] Among them, PEG has been most widely used for antifouling coatings owing to its flexibility, biocompatibility, and high degree of hydration.[15,16] It is well known that surfaces coated with PEG prevent protein adsorption and cell adhesion because of the large excluded hydrodynamic volume caused by surface-bound water molecules.[17]

Despite its excellent antifouling performance, PEG itself has limitations as a coating material for various surfaces due to the lack of reactive functional groups. Accordingly, several grafting strategies have been developed for its antifouling applications, including grafting-to and grafting-from approaches.[18] In the past decades, the grafting-from approach that initiates polymerization on surfaces was widely used because the formation of antifouling surfaces by surface-initiated polymerization could help achieve a high grafting efficiency.[19−21] Recently, the Benetti group demonstrated that copper-based surface-initiated atom transfer radical polymerization can facilitate the highly controlled synthesis of polymer brushes

Received: August 30, 2021
Revised: November 12, 2021
Published: November 24, 2021

https://doi.org/10.1021/acs.biomac.1c01124
Biomacromolecules 2021, 22, 5173−5184

Scheme 1. Simplified Schematic of the Antifouling Properties of Mussel-Inspired Catechol-Functionalized Multiloop Copolyethers. Different Polymer Topologies Lead to Different Antifouling Properties

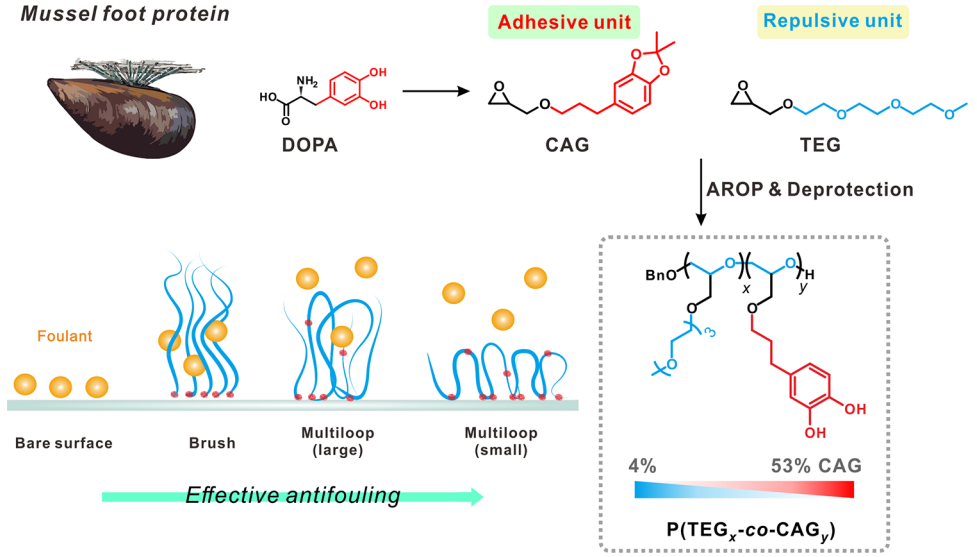

on large flat surfaces;[22] the resulting poly(2-methacryloyloxyethyl phosphorylcholine) brushes enabled the fabrication of highly lubricious coatings and biorepellent films. In contrast to the grafting-from approach, in which a reactive functional moiety is often necessary for anchoring the initiator, the grafting-to approach offers a convenient means to introduce well-defined polymers onto the surface without the need for a reactive functional moiety for anchoring the initiator. In this context, it is noteworthy that a surface-independent versatile surface coating based on the mussel-inspired L-3,4-dihydroxyphenylalanine has been exploited in various applications ranging from electronic to biomedical fields.[23]

Recently, surface-grafted polymer assemblies or polymer brushes have been widely employed as surface antifouling materials.[24−27] However, the existence of chain ends on polymer brushes often increases the interaction of foulants with the surface, which can lead to chain penetration and entanglement, which consequently degrade the antifouling properties. Polymer loops with low chain-end content have been suggested as an alternative owing to their large excluded volume and strong steric hindrance.[28] Earlier works have concentrated on the formation of loops by ABA triblock copolymers, in which the anchoring A-end block is connected with the antifouling B-midblock.[29] In this context, we have previously reported the superior antifouling properties of ABA-type triblock loop polymers functionalized with catechol moieties compared with an AB-type polymer brush.[30] More recently, studies on cyclic polymers without any chain end have led to the development of cyclic polymers with highly enhanced antifouling properties.[31−33] The morphology of a polymer (e.g., loop, brush, or cyclic) determines its antifouling and lubrication properties.[31] Despite these early examples of the successful realization of lubricious surfaces with cyclic polymers, few studies have investigated the effect of the loop dimension in multiloop polymers on the antifouling properties of the polymers.

Accordingly, in this study, we developed highly antifouling multiloop polyethers functionalized with a mussel-inspired catechol moiety. To explore the effect of the loop dimension on the antifouling properties within the framework of multiloop copolyethers, two types of functional monomers were exploited: catechol-acetonide glycidyl ether (CAG), a mussel-inspired catechol-based epoxide monomer, and triethylene glycol glycidyl ether (TEG), a hydrophilic antifouling epoxide monomer (Scheme 1). Specifically, a series of polyethers with different catechol contents were synthesized via anionic ring-opening polymerization (AROP) by using CAG and TEG to afford poly(TEG-*co*-CAG)$_n$. Subsequent deprotection allowed for the preparation of multiloop copolyethers with different numbers of anchoring groups at a fixed overall degree of polymerization (DP), resulting in different loop dimensions. The versatile adsorption and antifouling effects of multiloop polyethers were evaluated using atomic force microscopy (AFM), static contact angle measurements, and a quartz crystal microbalance with dissipation (QCM-D). Furthermore, the crucial role of the loop dimension in determining the antifouling properties was analyzed via a surface force apparatus (SFA) and a cell attachment assay.

MATERIALS AND METHODS

Materials. Triethylene glycol monomethyl ether, *p*-toluene sulfonic acid monohydrate (*p*-TsOH), lithium aluminum hydride ($LiAlH_4$), sodium hydroxide, epichlorohydrin (ECH), tetrabutylammonium bromide (TBAB), phosphazene base *t*-BuP_4 solution (0.80 M in hexane), bovine serum albumin (BSA), formaldehyde, phosphate-buffered saline (PBS, pH 7.4), and toluene were obtained from Sigma-Aldrich and used as received unless otherwise stated. 3,4-Dihyroxyhydrocinnamic acid (C-COOH), 2,2-dimethoxypropane, and aluminum oxide were purchased from Alfa Aesar, and 4′,6-diamidine-2′-phenylindole dihydrochloride (DAPI) and 5-chloromethylfluorescein diacetate were purchased from Thermo Fisher Scientific, USA. $CDCl_3$, D_2O, and MeOD were purchased from Cambridge Isotope Laboratories. All monomers used for polymerization were distilled over CaH_2.

Characterization. ^1H, ^{13}C, COSY, and in situ NMR were recorded on Bruker 400 and 900 MHz (Korea Basic Science Institute) spectrometers operating at room temperature by using $CDCl_3$, D_2O, and MeOD as the solvents. All spectra were measured using tetramethylsilane as an internal standard in the deuterated solvents. Size exclusion chromatography measurements were performed using an Agilent 1200 Series instrument with tetrahydrofuran (THF) as an

https://doi.org/10.1021/acs.biomac.1c01124
Biomacromolecules 2021, 22, 5173−5184

eluent at a flow rate of 1.0 mL/min at 40 °C. Surface morphologies of polymer-coated silicon surfaces were examined by AFM (NX10, Park Systems, Korea). The contact angle was determined using a Phoenix 300 goniometer (Surface Electro Optics Co. Ltd., Suwon, Korea). Surface interaction was studied using an SFA 2000 system (SurForce LLC, CA, USA). Real-time adsorption of the polymers and proteins was measured by a Q-sense E4 system (Biolin Scientific, Sweden). The mass and grafting density of each polymer adsorbed onto the surface were analyzed using QCM200 (Stanford Research Systems, CA, USA). FT-IR spectra were recorded on an Agilent Cary 630 FT-IR spectrometer equipped with an attenuated total reflectance module.

Synthesis of CAG. The catechol-functionalized monomer was prepared according to the method of Shin et al.[30] Yield: 73.5%. ^{1}H NMR (400 MHz, $CDCl_3$): δ [ppm] 6.72−6.53 (m, 3H), 3.72 (dd, J = 11.5, 3.0 Hz, 1H), 3.58−3.46 (m, 2H), 3.45−3.35 (m, 1H), 3.16 (m, J = 5.8, 4.0, 2.9 Hz, 1H), 2.81 (dd, J = 4.9, 4.3 Hz, 1H), 2.65−2.57 (m, 3H), 1.88 (m, J = 13.1, 6.4 Hz, 2H), 1.67 (s, 6H). ^{13}C NMR (100 MHz, $CDCl_3$): δ [ppm] 147.76, 145.83, 137.11, 135.06, 128.73, 120.61, 117.07, 108.76, 71.56, 70.08, 50.31, 43.18, 31.99, 31.76, 25.33.

Synthesis of TEG. A 250-mL round-bottom flask was charged with 40% NaOH solution (11.20 g of NaOH, 280 mmol), ECH (10.26 g, 111.00 mmol), and TBAB (0.45 g, 1.40 mmol). Triethylene glycol monomethyl ether was slowly added to the solution mixture by using a dropping funnel at 0 °C. The reaction was allowed to proceed for 18 h, and the progress was monitored by thin-layer chromatography. After the reaction was complete, the resulting solution was extracted using ethyl acetate, and the organic layers were dried over $MgSO_4$. The crude liquid product was purified by distillation after stirring over CaH_2. Yield: 86.8%. ^{1}H NMR (400 MHz, $CDCl_3$): δ [ppm] 7.28 (s, 1H), 7.28 (s, 1H), 3.81 (dd, J = 11.7, 3.1 Hz, 2H), 3.81 (dd, J = 11.7, 3.1 Hz, 2H), 3.69 (m, 17H), 3.61−3.53 (m, 4H), 3.50−3.38 (m, 8H), 3.21−3.15 (m, 2H), 2.81 (dd, J = 5.0, 4.2 Hz, 2H), 2.63 (dd, J = 5.0, 2.7 Hz, 2H), 1.72 (d, J = 8.2 Hz, 1H). ^{13}C NMR (100 MHz, $CDCl_3$): δ [ppm] 71.95, 71.89, 70.68, 70.56, 70.49, 60.26, 50.71, 44.13. ESI-MS (m/z): $C_{10}H_{20}O_5$ + Na ([M + Na]$^+$), calcd. 243.27, found 243.12.

In Situ ^{1}H NMR Polymerization Kinetics. A mixture of CAG (207.25 μg, 0.75 mmol), TEG monomer (165.20 μg, 0.75 mmol), and benzyl alcohol (3.12 μL, 0.030 mmol) in 0.50 mL toluene-d_8 was transferred to an NMR tube with a syringe, and the tube was sealed with a rubber septum. In order to obtain the initial position of each peak and the mole fraction of the monomers, we measured an initial sample at 0 h without t-BuP_4, and then the t-BuP_4 catalyst (0.80 M in hexane, 37.5 μL, 0.030 mmol) was added at the end to initiate the reaction. The sample temperature was set to 25 °C, and spectra were recorded every 10 min (total 25 scans in 250 min). The integral of the carbons of the monomers (δ = 51.62 ppm for CAG and 51.60 ppm for TEG) was monitored to calculate the monomer consumption, which was referenced to the residual signal of toluene (δ = 21.30 ppm).

Synthesis of P(TEG-*co*-CAG). A series of protected catechol functional copolyethers were synthesized by AROP by fixing the total DP at 50 and changing the molar ratio of the anchoring CAG moiety. The syntheses of all copolymers were carried out by the Schlenk technique under an Ar atmosphere in flame-dried glass tubes. Briefly, the synthesis of L53 was proceeded as follows: A mixture of t-BuP_4 (0.80 M in hexane, 0.11 mL, 0.09 mmol) and benzyl alcohol (9.44 μL, 0.09 mmol) in 1.81 mL toluene was stirred for 30 min. A mixture of TEG (0.50 g, 2.27 mmol) and CAG (0.60 g, 2.27 mmol) was then slowly added to the solution. As determined by ^{1}H NMR, the reaction was completed when the residual epoxide signals of the two monomers disappeared. After the confirmation of the reaction's completion, benzoic acid (11.09 mg, 0.09 mmol) was added and the solution was passed through neutral alumina oxide to remove the t-BuP_4 base. Finally, the solvent was evaporated to obtain poly(triethylene ethyl glycidyl ether-*co*-catechol-acetonide glycidyl ether), P(TEG$_{25}$-*co*-CAG$_{28}$). ^{1}H NMR (400 MHz, $CDCl_3$): δ [ppm] 6.59 (m, J = 16.5 Hz, 75H), 4.54 (s, 2H), 3.62−3.51 (m, 704H), 3.40 (s, J = 17.9 Hz, 84H), 2.56 (s, 50H), 1.81 (s, 50H), 1.65 (s, 168H). In the case of the block copolymer, the synthesis method was similar to the protocol described; instead, each monomer was added in sequence. The first TEG was added for the initiation, and the second monomer CAG was then added and the solution was stirred overnight to obtain poly(triethylene ethyl glycidyl ether-*block*-catechol-acetonide glycidyl ether), P(TEG$_{45}$-*b*-CAG$_5$). ^{1}H NMR (400 MHz, $CDCl_3$): δ [ppm] 6.56 (s, 15H), 4.53 (s, 2H), 3.38−3.55 (m, 845), 3.38 (s, 122H), 2.55 (s, 10H), 1.81 (s, 10H), 1.65 (s, 30H).

Removal of Acetonide Group. An amount of 200 mg of a protected copolyether sample (entry *L53 in Table 1) was stirred in 0.80 mL of 32% HCl solution and 9.20 mL of methanol at 40 °C. The mixture was stirred overnight and exposed to the atmosphere to allow acetone to escape. After stirring, the excess solvent was removed using a rotary evaporator. ^{1}H NMR (400 MHz, MeOD): δ [ppm] 6.64 (m, J = 31.2, 22.9 Hz, 75H), 4.54 (s, 2H), 3.70−3.40 (m, 704H), 3.37−3.32 (m, 84H), 2.53 (s, 50H), 1.80 (s, 50H).

Table 1. Characterizations of the Copolymers Synthesized in This Study

entry	polymer composition	F_{CAG}[a]	$M_{n,NMR}$[b] (g mol^{-1})	$M_{n,GPC}$[c] (g mol^{-1})	$Đ$[c]
*L4	P(TEG$_{48}$-*co*-CAG$_2$)	4	11,200	8700	1.07
*L10	P(TEG$_{45}$-*co*-CAG$_5$)	10	11,300	9300	1.06
*L20	P(TEG$_{40}$-*co*-CAG$_{10}$)	20	11,600	4000	1.11
*L53	P(TEG$_{25}$-*co*-CAG$_{28}$)	53	13,000	2900	1.15
*B10	P(TEG$_{45}$-*b*-CAG$_5$)	10	11,300	3800	1.11

[a]Molar ratio of the CAG monomer in the copolymers. [b]Determined via ^{1}H NMR spectroscopy in $CDCl_3$. [c]Determined from GPC measurements (THF, RI signal, and PEG standard) [*L(X) and *B(Y) indicate the protected polymers and their molar fraction of CAG monomer].

Interaction Force Measurements Via SFA. Freshly cleaved and back-silvered mica (Grade #1, S&J Trading, Floral Park, NY, USA) was used as the substrate, and it was glued onto a cylindrical glass disk (R = 2 cm) using an optical adhesive (NOA81, Norland Products, Inc. Cranbury, NJ, USA). To coat the polymer onto the mica surface, the polymer solution (5.0 mg/mL in 70% ethanol) was drop-cast on the mica surface for 30 min. The surface was then rinsed with 70% ethanol to remove weakly bound polymers and dried with nitrogen. Prepared surfaces were transferred into the SFA chamber with a cross-cylinder geometry, and 50 μL of the buffer was injected between opposing surfaces. The system was equilibrated for 1 h prior to the force−distance measurements. The approach and separation of two polymer-coated surfaces were performed with a speed of approximately 5 nm/s by a fine-controlled motor that was connected to the lower surface. The absolute distance (D) between the mica surfaces and interaction forces (F) was confirmed from fringes of equal chromatic order obtained using multiple beam interferometry and the spring deflection of a double cantilever spring (k = 2451.7 N/m). The measured forces were normalized by the radii of the cylindrical disks ($R \approx 2$ cm) as F/R. For the investigation of the antifouling properties of multiloop polyethers, BSA was chosen as the model foulant in this study. To investigate the antifouling performance of each polymer coating, we performed interaction force measurements in series by using four different intervening fluids: (i) 10 mM PBS at pH 7.4, (ii) BSA solution (0.50 mg/mL in 10 mM PBS), (iii) BSA solution (after 1 h of incubation), and (iv) 10 mM PBS rinse. Before the last force measurement with 10 mM PBS rinse, the surfaces were rigorously rinsed with deionized water to remove loosely bound BSA molecules. All experimental measurements were repeated at least thrice in a controlled environment (T = 23 °C). Three representative polymers (L4, L20, and L53) were selected to determine the correlation between the loop size and antifouling properties. The measured

https://doi.org/10.1021/acs.biomac.1c01124
Biomacromolecules 2021, 22, 5173−5184

Scheme 2. Preparation of (a) Two Functional Epoxide Monomers CAG and TEG and (b) Random Copolyethers (by using AROP) and Subsequent Deprotection under Acidic Conditions

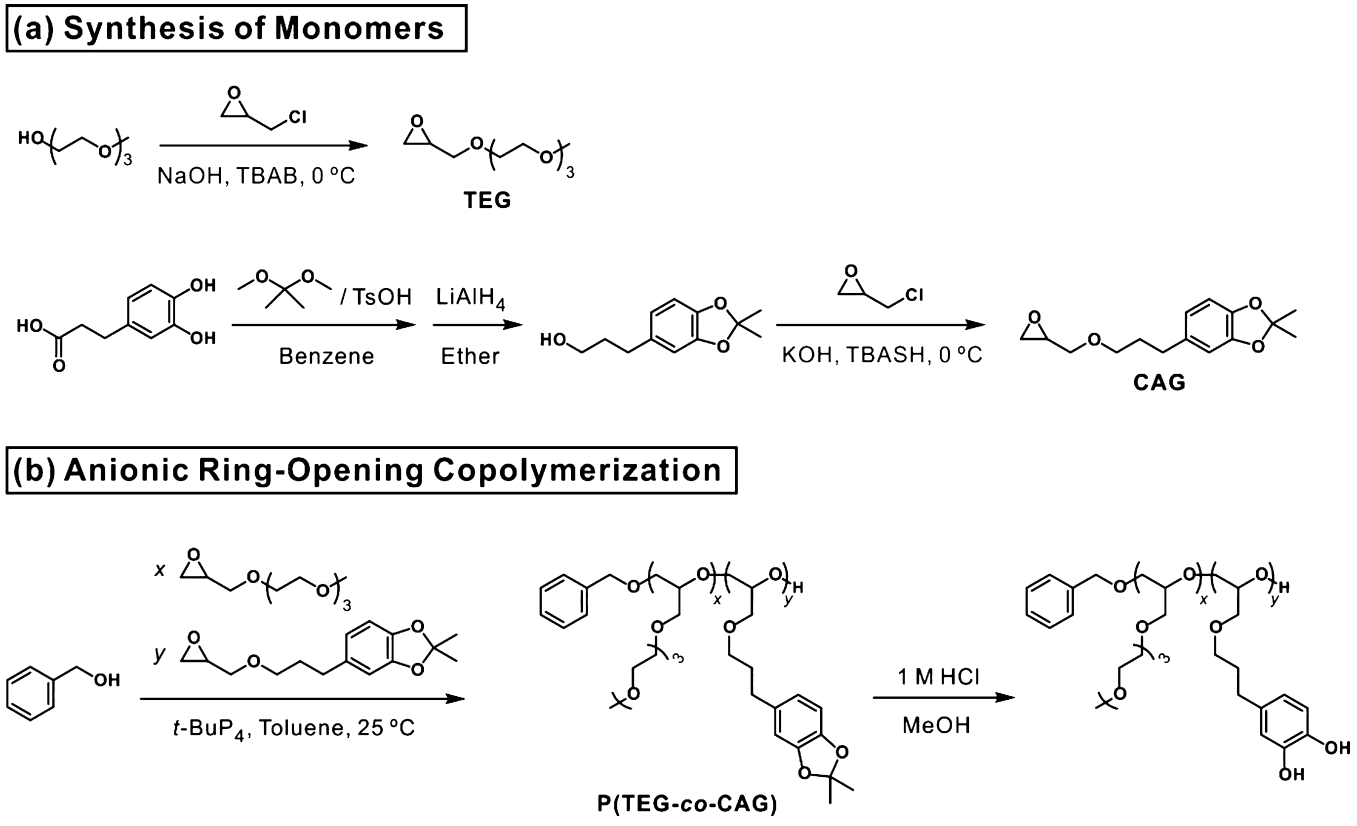

adhesion forces (F_{ad}, which is defined as the magnitude of the smallest F/R value) between two curved surfaces are converted to adhesion energy per unit area by using the Johnson−Kendall−Roberts model ($W_{ad} = F_{ad}/1.5\pi R$).[34]

Protein Adsorption Test Using QCM-D. Real-time surface adsorption was measured using a gold-coated sensor (QSX 301, Biolin Scientific). The sensor was transferred to a standard Q-sense flow module and equilibrated using 1× PBS (pH 7.4) before polymer coating. At 25 °C, the flow rate was fixed at 600 μL min^{-1} for all experiments. The Voigt model was used to calculate the mass of the adsorbed proteins and polymers in Qtools software (Q-Sense, Sweden). The density of the adsorbed BSA layer, fluid density, and fluid viscosity were assumed to be 1200 kg/m^3, 1000 kg/m^3, and 0.001 kg/ms, respectively. The grafting density (σ) was calculated using the relation $\sigma = mN_A/M_n$, where N_A is Avogadro's number and M_n is the number-average molecular weight of the polymer.

Static Contact Angle Measurement. The contact angle of a water droplet on the coated substrates was measured to analyze the surface characteristics of the substrates. Piranha solution (3:1 mixture of sulfuric acid and hydrogen peroxide) was used to clean the silicon wafer prior to its use. Each surface was incubated for 30 min in 5.0 mg/mL polymer solution in 70% ethanol at room temperature and then washed thrice with ethanol and dried with nitrogen. Each sample was measured five times, and the average value and standard deviation were calculated.

Cytotoxicity Assay. The fibroblast [e.g., human dermal fibroblast (HDF)] was used for the cell attachment test. Before the various evaluations, HDFs were stabilized by incubation at 37 °C in a humidified incubator with 5% CO_2 in Dulbecco's modified Eagle medium supplemented with 10% fetal bovine serum. After dip-coating each polymer over a poly(ethylene terephthalate glycol) (PETG) surface with an area of 1 cm × 1 cm, the loosely bounded polymers were washed with 70% ethanol. Each surface was thoroughly sterilized by exposure to UV radiation and transferred to a 24-well culture plate. The cell counting kit assay (CCK assay: D-Plus CCK cell viability assay kit, Dongin LS, Korea) was performed to monitor the cytotoxicity of HDFs with an initial seeding density of 2.0 × 10^4 cells/mL. Specifically, for both cases—when the HDFs were seeded immediately and after 48 h incubation—additional 10% (v/v) CCK assay solution was treated and incubated for 2 h. The relative viability was monitored by tracking the optical density at 450 nm. HDFs with a density of 2.0 × 10^4 cells/mL were incubated sufficiently for 48 h and subjected to hemocytometer-based cell counting.

In Vitro Cell Adhesion Assay. Polymer-coated PETG substrates were prepared as described above. An optical analysis (counter staining or bright-field images) was performed with the 48 h incubated HDFs (seeding density = 0.5 × 10^4 cells/mL). Before measurements, HDFs were fixed on the surfaces using 4% (v/v) formaldehyde for 15 min at room temperature. Subsequently, the cytoplasm of the fixed HDF was stained in green with 5 μM of 5-chloromethylfluorescein diacetate (CellTracker Green CMFDA) for 30 min, and the nucleus was stained in blue with 300 nM of 4′,6-diamidino-2-phenylindole. Counter-stained images were obtained with a confocal microscope (LSM 880, Carl Zeiss, USA). Furthermore, an optical microscope (IX51, Olympus) was used to obtain bright-field images.

RESULTS AND DISCUSSION

Design and Synthesis of Multiloop Polymers. Prior to the synthesis of the multiloop polymers, well-defined functional epoxide monomers were first designed and synthesized. A mussel-inspired catechol-based epoxide monomer, CAG, was prepared in three steps starting from 3-(3,4-dihydroxyphenyl)propionic acid by using a previously reported method.[30] The hydrophilic antifouling epoxide monomer, TEG was prepared from triethylene glycol monomethyl ether via a simple substitution reaction in high yield (86%) (Scheme 2). The successful syntheses of the respective monomers were

https://doi.org/10.1021/acs.biomac.1c01124
Biomacromolecules 2021, 22, 5173−5184

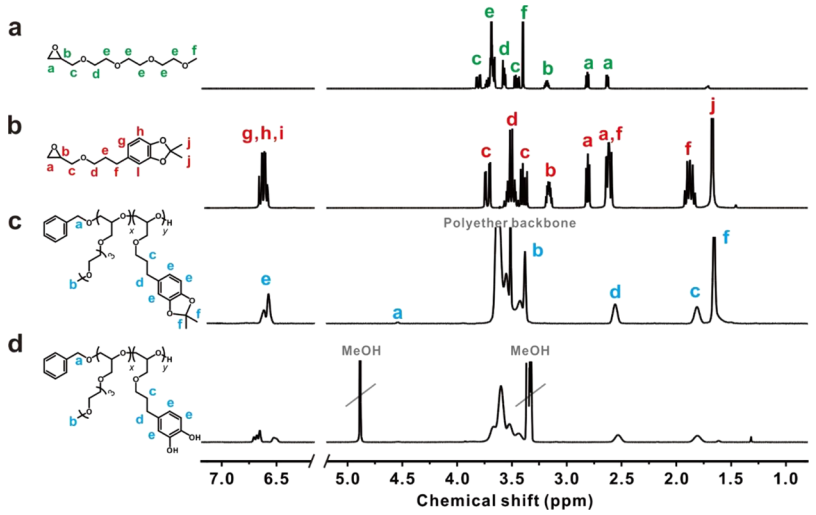

Figure 1. Representative ^{1}H NMR spectrum of (a) TEG monomer, (b) CAG monomer, (c) multiloop P(TEG$_{25}$-*co*-CAG$_{28}$) polyether (entry *L53 in Table 1), and (d) after deprotection of P(TEG$_{25}$-*co*-CAG$_{28}$) polyether. All spectra were collected in $CDCl_3$ except (d) in MeOD.

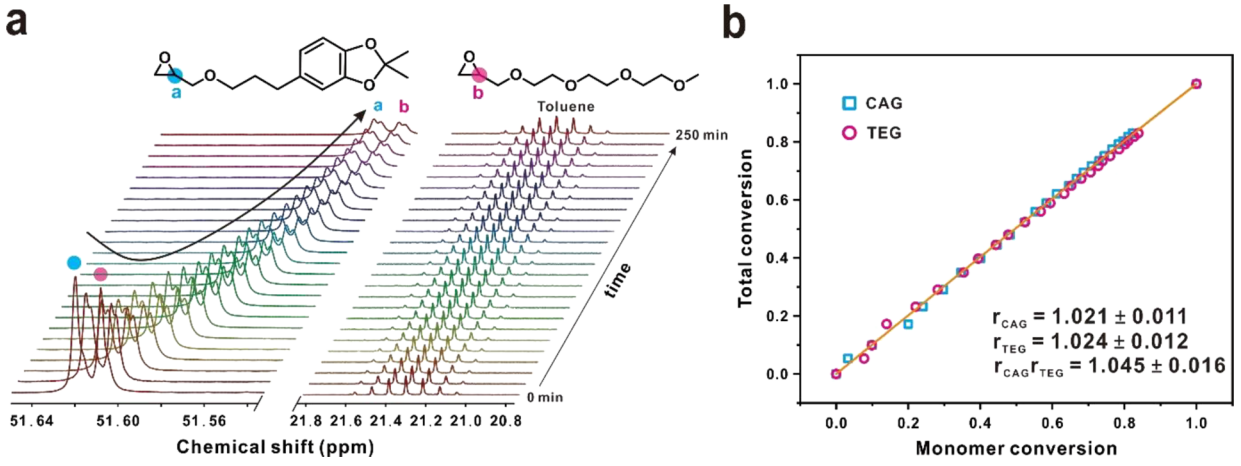

Figure 2. (a) Time-resolved in situ ^{13}C NMR spectra of copolymerization of CAG and TEG in toluene-d_8 under polymerization conditions at 27 °C. (b) Plot of total polymerization conversion versus monomer conversion for the copolymerization of CAG (blue square) and TEG (red circle). The initial monomer compositions were n_{CAG} = 0.54 and n_{TEG} = 0.46.

confirmed via various NMR techniques, including ^{1}H, ^{13}C, and COSY spectroscopy, and ESI-MS spectrometry (Figure 1 and Figures S1−S5 in the Supporting Information). Each monomer was purified by column chromatography and vacuum distillation prior to its polymerization.

After the synthesis of the two epoxide monomers, a series of random copolyethers, P(TEG-*co*-CAG), were prepared via AROP. Using benzyl alcohol as an initiator, we used the highly basic organic phosphazene base *t*-BuP$_4$ in toluene at room temperature. The organic superbase *t*-BuP$_4$ was chosen, as it facilitates controlled polymerization under mild conditions, as demonstrated in a previous study.[30] Random copolymers with different TGE and CAG contents were prepared (Table 1) at a fixed overall DP = 50. In particular, the fraction of CAG moiety was increased from 4 to 50% to introduce a more adhesive moiety while modulating the loop dimension once anchored on the surface. As a control, a brush-like diblock copolymer, P(TEG-*b*-CAG), was prepared via the sequential addition of the appropriate monomer under identical reaction conditions, except for the sequential addition of monomers (Figure S6). In all cases, the AROP of the two monomers was successful, achieving over 99% conversion within 12 h.

As shown in Figure 1d, the ^{1}H NMR spectra of the copolyethers showed characteristic peaks corresponding to the respective monomers, for example, the benzylic proton of the initiator (*a*, 4.50−4.55 ppm), the methoxy group of TEG (*b*, 3.34−3.38 ppm), the aromatic ring (*e*, 6.50−6.65 ppm), acetonide group on the catechol moiety in CAG (*f*, 1.61−1.67 ppm), and the polyether backbone (3.33−3.58 ppm). All copolyethers were then subjected to deprotection with hydrochloric acid, which liberated the free catechol groups in the acetonide-protecting group on the CAG moiety. The completion of deprotection was confirmed by ^{1}H NMR, with the disappearance of the acetonide peak in the resulting copolyethers (Figure 1d). Furthermore, FT-IR spectra revealed the appearance of a broad hydroxyl peak at 3500 cm^{-1} (Figure S7).

The characterizations of the synthesized polymers are presented in Table 1. The molecular weight determined by gel permeation chromatography (GPC) was relatively smaller than the value obtained from ^{1}H NMR spectroscopy owing to the increase in the hydrophobicity with the catechol ratio (Figure S8). The hydrophobic catechol units of the homopolymer could have collapsed in THF because of its

https://doi.org/10.1021/acs.biomac.1c01124
Biomacromolecules 2021, 22, 5173−5184

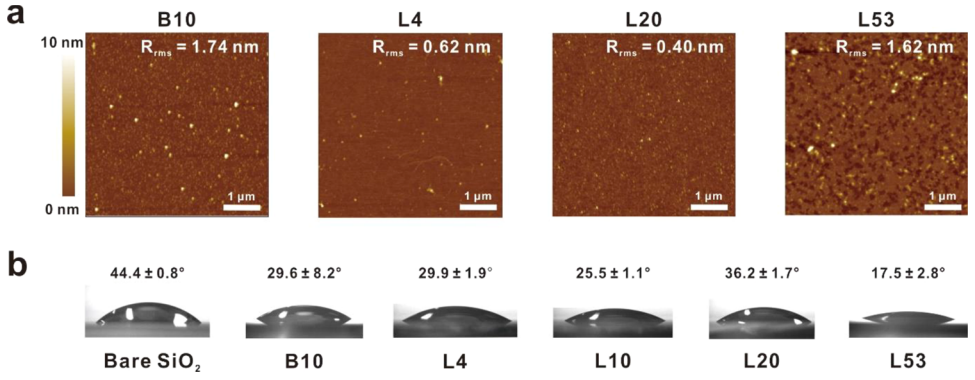

Figure 3. (a) Representative topographic AFM images of polymer coatings on a silicon wafer (polymer conc. of 5.0 mg/mL in 70% EtOH). The root-mean-squared roughness (R_{rms}) value was determined from the average of three independent measurements. (b) Static contact angles of water droplets on each substrate coated with polymers. The average contact angle value for five repetitions is reported along with the standard deviation.

higher polarity than the homopolymer, which can lead to a difference in their hydrodynamic volumes.[35] However, the narrow range of the molecular weight distributions ($Đ$ = 1.07−1.11) confirms the successful synthesis of the copolyethers at the fixed total DP of 50.

The reactivity ratios of CAG and TEG during copolymerization were compared to reveal the microstructure of the P(TEG-*co*-CAG) copolymers. Specifically, the copolymerization of CAG and TEG was monitored using in situ ^{13}C NMR spectroscopy with inverse-gated decoupling (Figure 2a). In particular, the integration values of the methine peaks of the respective CAG and TEG monomers were used to calculate the monomer conversion in reference to the signal from toluene (21.3 ppm) as an internal standard. As shown in Figure 2b, the total conversion ratio of both monomers was plotted against the overall monomer conversion ratio. By employing the nonterminal model of chain copolymerization developed by Lynd and co-workers,[36] the reactivity ratios of the monomers were found to be r_{CAG} = 1.021 ± 0.011 and r_{TEG} = 1.024 ± 0.012, indicating almost ideal statistical copolymerization (Figure 2b). This similarity in the reactivity ratio is important, in that the copolymerization between the two monomers allows for the random incorporation of the adhesive moiety along the backbone in the multiloop copolyethers. In other words, the topology of the polymer multiloops can be controlled simply by varying the ratio of the anchoring groups without requiring complicated synthetic methods.

Surface Characterizations of Polymer Coatings. Subsequently, the deprotected copolyethers were coated on a silicon wafer (used as a model substrate) via a solution dipping method. The morphology of the polymer-coated surfaces was investigated by AFM (Figure 3a). The surface morphology of all polymers was relatively uniform with occasional observation of the globular structures on the surfaces. The roughness was determined by scanning the horizontal axis over the entire surface. For example, the root-mean-squared roughness (R_{rms}) of B10 was determined to be 1.7 nm (averaged over an area of 5.0 μm^2), while the multiloop polymers L4 and L20 showed lower R_{rms} values and a smooth surface. Interestingly, a higher R_{rms} value of 1.6 nm was observed in the case of L53, which could be attributed to aggregates formed from inter- and intramolecular hydrogen bonding (H-bonding) between the catechol moiety (H-bonding donor) and the polyether backbone and/or the side chain of the triethylene glycol moiety (H-bonding acceptors) in the multiloop copolyethers. It is also noteworthy that acetonide protected polymers prior to the deprotection was readily rinsed away, which indicated the critical role of the free catechol moiety in the anchoring of the polymers on the substrate.

In addition, the versatile surface binding capability of the polymers was examined by measuring the static contact angle of water droplets after coating the substrate with the prepared polymers (Figure S9). While the bare silicon wafer showed a static contact angle of 44°, the polymer-coated substrates displayed a reduced contact angle of 17.5−36.2° in general, demonstrating the potential of surface hydration with the prepared polymers.

Interaction Force Measurement with SFA. The SFA, which has been widely used to measure physical interaction forces between macroscopic surfaces,[37] was used to determine the polymer film thickness and the antifouling properties of each copolyether coated surfaces. The force−distance measurements were obtained between polymer-coated mica surfaces (Figure 4). The measured force−distance profiles provide two important parameters, from which the antifouling properties can be ascertained: (i) the change in the steric wall thickness (D_{sw}, defined as D at F/R = 60 mN/m) and (ii) the change in the adhesion/repulsion force, before and after BSA injection and washing. In the SFA analysis, it is assumed that all polymers coat the surface uniformly in a single layer with rigorous rinsing steps and that the two polymer-coated surfaces do not exchange attractive force.

Under the fluidic PBS environment, the measured D_{sw} of L4 and L20 polymers was 4.72 and 5.17 nm, respectively, while for L53 with the highest catechol group content, D_{sw} was 2.21 nm, indicating the smallest loop size as anticipated. Furthermore, all the multiloop polymers exhibited purely repulsive force−distance profiles during approach, mostly because of the steric repulsion between the highly hydrated polyether backbones of the coated polymers.[37] After BSA injection, increases in the repulsive force and D_{sw} between the multiloop coated surfaces were observed for all copolyethers tested, indicating the adsorption of BSA molecules on the polymer surfaces and the generation of additional steric repulsion between surfaces. Furthermore, after incubation for 1 h in BSA solution, D_{sw} significantly increased for each copolyether because of the additional adsorption of BSA owing to strong hydrophobic interactions.[36] Finally, after rinsing the surfaces with deionized water, force−distance profile measurements in PBS showed that the L20 sample had recovered its original thickness and adhesion, which indicated the successful antifouling behavior of the multiloop polymer coating. The other two samples

https://doi.org/10.1021/acs.biomac.1c01124
Biomacromolecules 2021, 22, 5173−5184

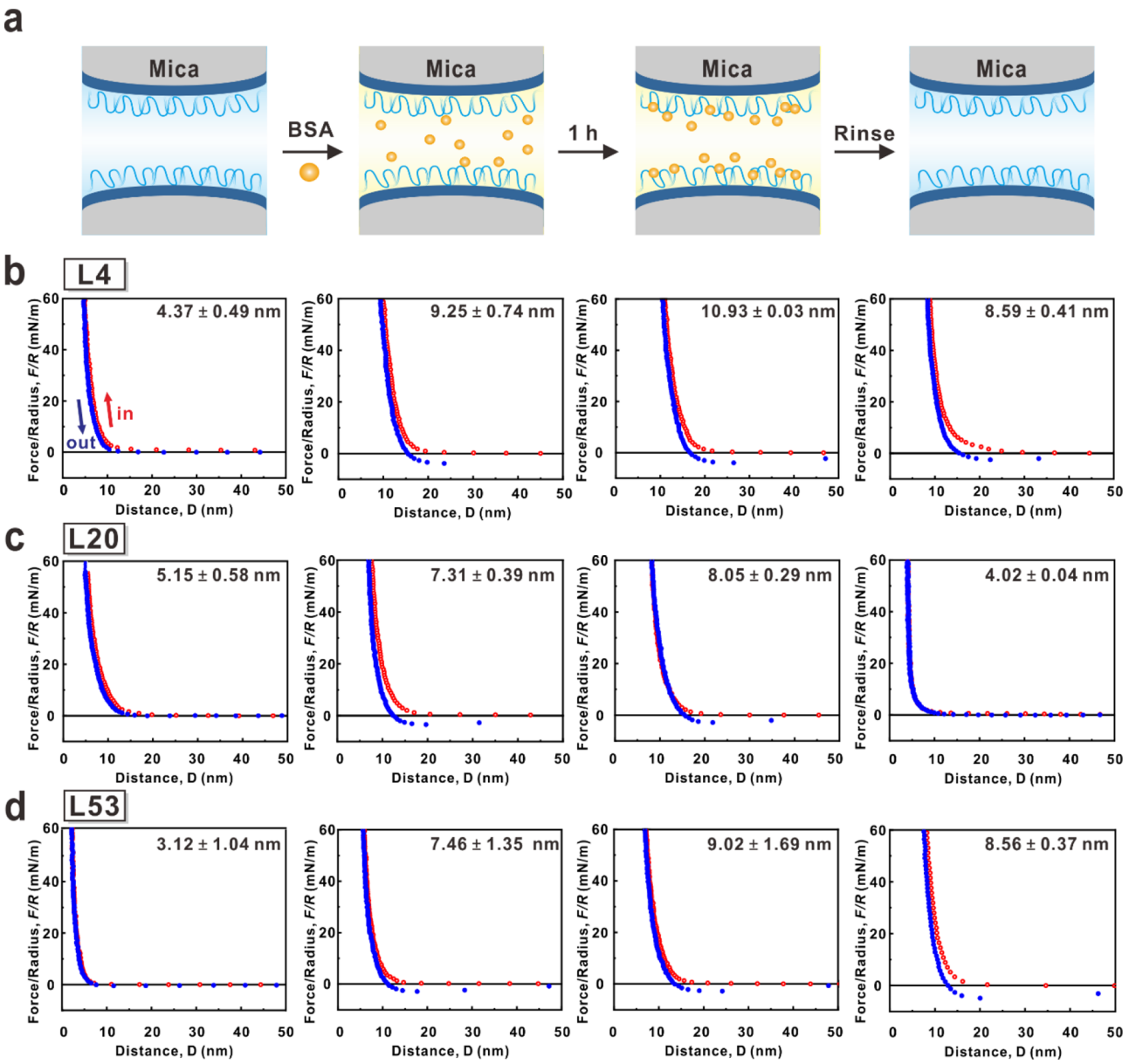

Figure 4. (a) Schematics depicting the antifouling evaluation of the polymer coatings with an SFA and (b–d) representative force–distance profiles between two polymer-coated surfaces of (b) L4, (c) L20, and (d) L53 polymer samples with the following treatment sequences (from left to right panel): polymer coating in 10 mM PBS, introduction of BSA solution, after 1 h incubation of BSA, and rinsed with deionized water. The number in each panel represents the steric wall thickness (D_{sw}).

appeared to partially recover their original thickness after the rinsing process. However, they did not fully recover their initial thickness due to the trapping of the BSA within the multiloop polymers.

By monitoring the adhesion force during each step, we can further evaluate the effectiveness of the antifouling properties. For instance, all samples showed low adhesion after BSA injection followed by incubation for 1 h. The initial adhesion energy slightly decreased with increasing CAG content (0.83 ± 0.01 and 0.52 ± 0.09 mJ/m^2 for L4 and L53, respectively), which was mediated by bridging of the BSA molecules that penetrated between surfaces coated with different multiloop polymers. The adhesion energy observed after initial BSA injection onto the polymer-coated surface (i.e., pre-wash D_{sw}) is slightly different from that appears after complete washing with PBS (i.e., post-wash D_{sw}). Interestingly, for the final adhesion, the L20 sample indicated the complete disappearance of surface adhesion after rigorous washing with PBS, while the L4 and L53 samples retained adhesion forces of 0.41 and 0.40 mJ/m^2 between surfaces, respectively. Taken together with the complete recovery of the D_{sw} value in L20, the purely repulsive force after washing indicates that L20 possessed the best antifouling properties among the samples under SFA measurement conditions.

Independent of the polymer thickness measured by using the SFA, we compared the thickness values of the polymers using ellipsometry (Figure S10). The reason that the thickness measured by using the SFA differed from that obtained using ellipsometry was the wet state of the polymer loop. In the case of the SFA measurement, the loop was in a wet state and because the catechol was strongly attached to the surface,

https://doi.org/10.1021/acs.biomac.1c01124
Biomacromolecules 2021, 22, 5173–5184

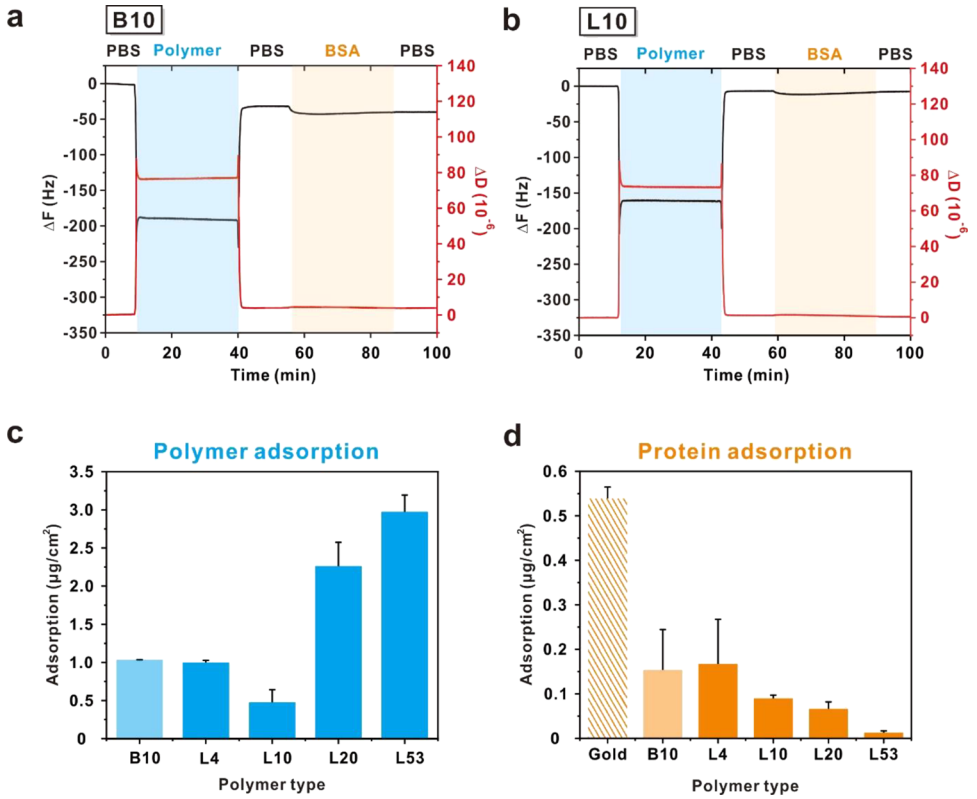

Figure 5. (a, b) Changes in the frequency (black) and dissipation (red) associated with the (a) brush B10 polymer and (b) multiloop L10 polymer coated on a gold substrate, obtained from QCM-D measurements. A series of antifouling assessment protocols were performed. (c) Adsorption of the various polymer samples on bare gold surfaces. (d) Adsorption of BSA on various polymer samples coated on bare gold surfaces. For each experiment, three overtones with more than three repetitions were used to report the average values along with the standard deviation.

water molecules could pass freely through the loop, resulting in a larger thickness.

Adsorption of the Polymer and Protein. To quantitatively analyze the real-time antifouling performance by obtaining the mass of the coated polymers and the proteins adsorbed onto the surfaces, we employed QCM-D analysis (Figure 5). Prior to the coating of the polymers, the bare gold substrate was equilibrated in flowing PBS buffer at pH 7.4 for obtaining steady frequency and dissipation baselines. Polymer coating was then performed using the polymer solution (5.0 mg/mL in 70% ethanol) for 30 min, which generated a negative frequency shift, suggesting an increase in the mass of the substrate after polymer coating. During the injection of the polymer solution, the steep slopes of the ΔD versus $\Delta F/n$ plot of each polymer (for example 3.7×10^{-7}/Hz for B10 and 4.2×10^{-7}/Hz for L10 samples) showed that the adsorbates on the substrate possessed viscoelastic properties (Figures S11−S15) as similarly reported.[29] Accordingly, the Voigt model was used instead of the conventional Sauerbrey equation in this study to calculate the mass of the polymer deposited.

After the coating of the polymers, the loosely bound polymers were removed by an additional PBS rinsing process, and it was followed by the injection of BSA solution into the polymer-coated substrates. Because the baselines of each section were constant under the continuous flow rate, it was confirmed that the catechol-functionalized copolyethers were successfully coated on the gold substrate, as expected. As the CAG content of the multiloop polymers increased, the amount of the adsorbed polymer increased from 997.84 ng/cm^2 for L4 to 2974.24 ng/cm^2 for L53, possibly because of the increased number of anchoring sites on the surface (Figure 5c). It is also noteworthy that the coating stability of all catechol-functionalized copolyethers were maintained even under conditions of a continuous flow rate (0.60 mL/min).

Finally, the mass of the adsorbed BSA was measured after the initial BSA solution injection. In the case of the bare gold substrate, the mass of the adsorbed BSA (536.15 ng/cm^2) was significantly higher than that of B10 (153.86 ng/cm^2), L10 (89.94 ng/cm^2), and L53 (12.85 ng/cm^2). A comparison of the brush and loop topologies showed that L10 showed lower protein adsorption than B10, in agreement with the result of our previous investigation, in which AB-type brush and ABA-type loop polymers with a PEG spacer as an antifouling segment were compared.[30]

In the context of the series of multiloop polyethers, the adsorption of the BSA decreased as the number of anchoring groups increased, in the order of L4, L10, L20, and L53. It is noteworthy that the hydrophilic TEG moiety in the side chains was sufficient to provide a level of antifouling effects similar to that provided by the PEG segment to prohibit proteins from binding onto the multiloop polymer-coated surfaces. The content of catechol within a polymer can play a critical role in modulating the loop dimension. For example, upon increasing the surface-anchoring CAG moiety content from L4 to L53 in the multiloop polymers, smaller loops with a short, exposed tail will be generated, which in turn will result in less protein adsorption. The presence of a smaller loop dimension in a multiloop polymer with a higher catechol content was further corroborated by D_{sw} determined with the SFA (Figure 4). Although the general trend was in line with the results

https://doi.org/10.1021/acs.biomac.1c01124
Biomacromolecules 2021, 22, 5173−5184

Table 2. Antifouling Properties of the Copolymers Investigated in This Study

entry		QCM-D[a]			SFA[b]	
					adhesion energy (mJ/m^2)	
	polymer composition	polymer adsorption (ng/cm^2)	BSA adsorption (ng/cm^2)	σ (chains/nm^2)	pre-wash	post-wash
B10	P(TEG_{45}-*b*-CAG_5)	1034.88 ± 1.81	153.86 ± 90.90	0.56	ND	ND
L4	P(TEG_{48}-*co*-CAG_2)	997.84 ± 28.63	167.52 ± 100.01	0.55	0.83 ± 0.01	0.41 ± 0.17
L10	P(TEG_{45}-*co*-CAG_5)	475.45 ± 167.35	89.94 ± 7.32	0.23	ND	ND
L20	P(TEG_{40}-*co*-CAG_{10})	2017.26 ± 32.71	77.56 ± 31.58	1.23	0.56 ± 0.07	0
L53	P(TEG_{25}-*co*-CAG_{28})	2974.24 ± 219.99	12.85 ± 4.01	1.52	0.52 ± 0.09	0.40 ± 0.30

[a]The adsorbed mass and grafting density was measured by substituting the frequency into the Voigt model and averaging the values twice. Each polymer and protein were coated at a concentration of 5.0 mg/mL for 30 min and washed with PBS. [b]Three representative samples based on the equivalent of catechol were measured to confirm the size of the loops. The values for L4, L20, and L53 are reported with a mean with standard deviation (n = 2, 4, and 7). Other samples which were not measured is expressed as ND (not determined). Pre-wash and post-wash correspond to the values collected for BSA adsorption before and after final PBS rinsing, respectively.

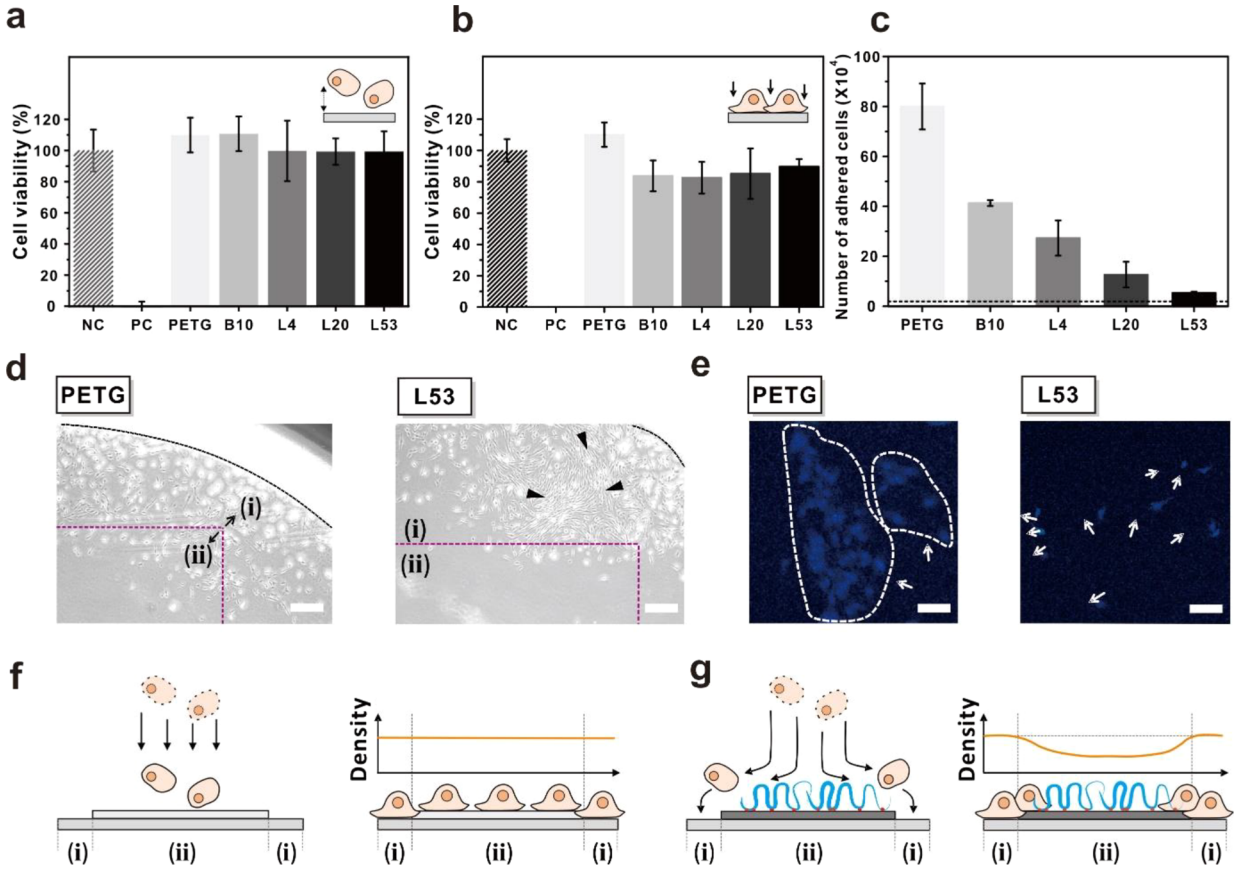

Figure 6. In vitro evaluation of the antifouling properties of the brush and multiloop polymers. (a, b) Cellular viability of (a) floating and (b) adhered human dermal fibroblast (HDF). NC (negative control) refers to the cells grown in the absence of polymers, and PC (positive control) refers to the cells treated with DMSO. (c) Number of cells grown on the PETG surface and polymer-coated surfaces. The black dashed line indicates the initial seeding density (i.e., 2.0 × 10^4 cell/mL). (d) Optical images of the HDFs distributed on each surface. Regions (i) and (ii) distinguish the pristine and the L53-coated PETG substrates, respectively. (e) Fluorescence microscopy images of DAPI-stained fibroblasts, which are indicated by white arrows over each sample. (f, g) Schematic of the proposed antifouling mechanism of (f) bare and (g) multiloop L53-coated surface. All values are reported a mean with the standard deviation (n = 3). Each scale bar corresponds to 200 μm.

collected using the SFA, there was a subtle difference: the amount of protein adsorption was the least in the case of L53, unlike the case of SFA. As mentioned earlier in the discussion of the surface morphology of the L53-coated surfaces, there could be a formation of multilayered copolyether layers owing to contributions from the inter- and intramolecular H-bonding between the catechol moiety (H-bonding donor) and the polyether backbone and/or the side chain of the TEG moiety (H-bonding acceptors); the contributions become more pronounced, particularly in the case of higher catechol content, as in the case of L53. Furthermore, the limited flow rate available for the QCM-D measurement compared with the rigorous washing steps (e.g., splashing with a water gun) involved in SFA measurement could contribute to the observed differences in the multilayer formation in the L53 polymer. It is also of note that the difference in the catechol-substrate interaction is not significant, considering the versatile surface-independent adhesive nature of the catechol chemistry.

https://doi.org/10.1021/acs.biomac.1c01124
Biomacromolecules 2021, 22, 5173−5184

From the absorbed polymer mass, we compared the grafting density (σ) of each polymer (Table 2). Comparing the B10 (block) and L10 (random) samples with an identical number of anchoring groups, we observed that the antifouling properties were relatively higher in L10 than B10, despite the low grafting density of L10 (0.26 chains/nm^2) compared with B10 (0.56 chains/nm^2). By comparing polymers of the same composition, we could confirm that the topology had a large effect on the antifouling properties owing to the low chain end exposure in the loop polymer. In the context of the series of multiloop polymers, the grafting density generally increased with the number of anchoring groups owing to the enhanced number of anchoring moieties on the surfaces.

Biofouling and Cytotoxicity Assay. Encouraged by the successful realization of antifouling properties in the multiloop random copolyethers, we further evaluated their cytotoxicity on HDF for achieving a wider scope of applications (Figure 6). All polymers were dip-coated on PETG substrates for 30 min for in vitro assay. We chose PETG as the representative substrate in this study because it is one of the most commonly used plastics in dental materials for its high biocompatibility, mechanical strength, and resistance against chemicals.[38]

Initially, the polymer-coated substrates were placed in the 24-well plate, and HDFs were seeded immediately and for 48 h to monitor the cytotoxicity and antifouling properties of each sample. The in vitro cytotoxicity of each polymer-coated substrate was assessed via the CCK assay, and considerable cellular compatibility was observed toward both floating and adhered fibroblasts (Figure 6a,b). Separately, when the number of the cells grown on the polymer-coated PETG surfaces were compared, all polymer-coated surfaces were found to retain a significantly reduced number of cells, clearly demonstrating the antifouling performance of the brush and multiloop polymers. It was noticeable that as the fraction of the anchoring group increased from L4 to L53 in the multiloop polymers (i.e., the loop dimension decreases), the antifouling performance improved, in good agreement with the results from QCM-D measurements (Figure 6c). In particular, the total number of adhered fibroblasts was significantly reduced in the case of the L53-coated PETG. While the fibroblasts showed normal adhesion and proliferation on an uncoated surface, most cells deposited on the multiloop L53 polymer-coated surface were found to be small and were not colonized, as revealed by optical and fluorescence microscopy images (Figure 6d,e). On the basis of this observation, one can propose an antifouling mechanism, in which the cells slide over the hydrated multiloop polymers on the surface of PETG, resulting in the observed antifouling performance (Figure 6f,g).

CONCLUSIONS

In summary, a series of multiloop random copolyethers were designed and prepared by using two functional epoxide monomers, TEG and CAG, to explore the topology effect on the antifouling properties. On the basis of the random nature of the polymers, loop topology could be simply controlled in a one-pot reaction by changing the number of anchoring groups, while fixing the total DP. The hydrophilic backbone and side chain of the polymers could impart antifouling effects, while making strong, stable adhesion to the surface. Further investigation, from micro- to macroscopic antifouling experiments, confirmed that the loop size could be adjusted by varying the number of anchoring sites and the antifouling effects could vary depending on the type of substrates and external coating conditions. Together with its excellent cell viability, this study provides a simple way to control the polymer topology and antifouling properties.

ASSOCIATED CONTENT

Supporting Information

The Supporting Information is available free of charge at https://pubs.acs.org/doi/10.1021/acs.biomac.1c01124.

Additional ^{1}H, ^{13}C NMR, ESI-MS, FT-IR, and GPC data of the polymers and contact angle and QCM-D slope plot of the multiloop series (PDF)

AUTHOR INFORMATION

Corresponding Authors

Dong Woog Lee − *School of Energy and Chemical Engineering, Ulsan National Institute of Science and Technology (UNIST), Ulsan 44919, Republic of Korea;* orcid.org/0000-0002-1572-9270; Email: dongwoog.lee@unist.ac.kr

Byeong-Su Kim − *Department of Chemistry, Yonsei University, Seoul 03722, Republic of Korea;* orcid.org/0000-0002-6419-3054; Email: bskim19@yonsei.ac.kr

Authors

Suebin Park − *Department of Chemistry, Yonsei University, Seoul 03722, Republic of Korea;* orcid.org/0000-0002-4677-076X

Minseong Kim − *Department of Chemistry, Yonsei University, Seoul 03722, Republic of Korea; Department of Chemistry, Ulsan National Institute of Science and Technology (UNIST), Ulsan 44919, Republic of Korea;* orcid.org/0000-0002-2612-922X

Jinwoo Park − *School of Energy and Chemical Engineering, Ulsan National Institute of Science and Technology (UNIST), Ulsan 44919, Republic of Korea;* orcid.org/0000-0003-2921-2923

Woojin Choi − *Department of Chemical and Biomolecular Engineering, College of Engineering, Yonsei University, Seoul 03722, Republic of Korea;* orcid.org/0000-0002-5886-8836

Jinkee Hong − *Department of Chemical and Biomolecular Engineering, College of Engineering, Yonsei University, Seoul 03722, Republic of Korea;* orcid.org/0000-0003-3243-8536

Complete contact information is available at: https://pubs.acs.org/10.1021/acs.biomac.1c01124

Notes

The authors declare no competing financial interest.

ACKNOWLEDGMENTS

This work was supported by Samsung Research Funding & Incubation Center of Samsung Electronics under Project Number SRFC-MA1602-07 and the Yonsei University Research Fund of 2020 (2020-22-0494).

REFERENCES

(1) Ratner, B. D.; Bryant, S. J. Biomaterials: Where We Have Been and Where We Are Going. *Annu. Rev. Biomed. Eng.* **2004**, *6*, 41−75.
(2) Jiang, S.; Cao, Z. Ultralow-Fouling, Functionalizable, and Hydrolyzable Zwitterionic Materials and Their Derivatives for Biological Applications. *Adv. Mater.* **2010**, *22*, 920−932.

(3) Yang, C.; Ding, X.; Ono, R. J.; Lee, H.; Hsu, L. Y.; Tong, Y. W.; Hedrick, J.; Yang, Y. Y. Brush-Like Polycarbonates Containing Dopamine, Cations, and PEG Providing a Broad-Spectrum, Antibacterial, and Antifouling Surface via One-Step Coating. *Adv. Mater.* **2014**, *26*, 7346−7351.
(4) Goh, S. C.; Luan, Y.; Wang, X.; Du, H.; Chau, C.; Schellhorn, H. E.; Brash, J. L.; Chen, H.; Fang, Q. Polydopamine−Polyethylene Glycol−Albumin Antifouling Coatings on Multiple Substrates. *J. Mater. Chem. B* **2018**, *6*, 940−949.
(5) Gudipati, C. S.; Finlay, J. A.; Callow, J. A.; Callow, M. E.; Wooley, K. L. The Antifouling and Fouling-Release Perfomance of Hyperbranched Fluoropolymer (HBFP)−Poly(ethylene glycol) (PEG) Composite Coatings Evaluated by Adsorption of Biomacromolecules and the Green Fouling AlgaUlva. *Langmuir* **2005**, *21*, 3044−3053.
(6) Li, L.; Yan, B.; Zhang, L.; Tian, Y.; Zeng, H. Mussel-inspired Antifouling Coatings Bearing Polymer Loops. *Chem. Commun.* **2015**, *51*, 15780−15783.
(7) Morgese, G.; Gombert, Y.; Ramakrishna, S. N.; Benetti, E. M. Mixing Poly(ethylene glycol) and Poly(2-alkyl-2-oxazoline)s Enhances Hydration and Viscoelasticity of Polymer Brushes and Determines Their Nanotribological and Antifouling Properties. *ACS Appl. Mater. Interfaces* **2018**, *10*, 41839−41848.
(8) Tang, P.; di Cio, S.; Wang, W.; Gautrot, J. E. Surface-Initiated Poly(oligo(2-alkyl-2-oxazoline)methacrylate) Brushes. *Langmuir* **2018**, *34*, 10019−10027.
(9) Tauhardt, L.; Kempe, K.; Gottschaldt, M.; Schubert, U. S. Poly(2-oxazoline) Functionalized Surfaces: from Modification to Application. *Chem. Soc. Rev.* **2013**, *42*, 7998−8011.
(10) Riyasudheen, N.; Paul, M. J.; Sujith, A. Effect of Poly(vinyl pyrrolidone) on Antifouling Properties of Asymmetric Poly(ethylene-co-vinyl alcohol) Membranes. *Chem. Eng. Technol.* **2014**, *37*, 1021−1029.
(11) Guo, H.; Chen, P.; Tian, S.; Ma, Y.; Li, Q.; Wen, C.; Yang, J.; Zhang, L. Amphiphilic Marine Antifouling Coatings Based on a Hydrophilic Polyvinylpyrrolidone and Hydrophobic Fluorine−Silicon-Containing Block Copolymer. *Langmuir* **2020**, *36*, 14573−14581.
(12) Jiang, J.; Zhu, L.; Zhu, L.; Zhang, H.; Zhu, B.; Xu, Y. Antifouling and Antimicrobial Polymer Membranes Based on Bioinspired Polydopamine and Strong Hydrogen-Bonded Poly(N-vinyl pyrrolidone). *ACS Appl. Mater. Interfaces* **2013**, *5*, 12895−12904.
(13) Wiarachai, O.; Vilaivan, T.; Iwasaki, Y.; Hoven, V. P. Clickable and Antifouling Platform of Poly[(propargyl methacrylate)-ran-(2-methacryloyloxyethyl phosphorylcholine)] for Biosensing Applications. *Langmuir* **2016**, *32*, 1184−1194.
(14) Guo, H.; Liu, X.; Zhao, W.; Xie, C.; Zhu, Y.; Wen, C.; Li, Q.; Sui, X.; Yang, J.; Zhang, L. A Polyvinylpyrrolidone-based Surface-active Copolymer for an Effective Marine Antifouling Coating. *Prog. Org. Coat.* **2021**, *150*, No. 105975.
(15) Liu, L.; Li, W.; Liu, Q. Recent Development of Antifuling Polymers: Structure, Evaluation, and Biomedical Applications in Nano/Micro-Structures. *WIREs Nanomed. Nanobiotechnol.* **2014**, *6*, 599−614.
(16) Krishnan, S.; Weinman, C. J.; Ober, C. K. Advances in Polymers for Anti-biofouling Surfaces. *J. Mater. Chem.* **2008**, *18*, 3405−3413.
(17) Leng, C.; Hung, H.-C.; Sun, S.; Wang, D.; Li, Y.; Jiang, S.; Chen, Z. Probing the Surface Hydration of Nonfouling Zwitterionic and PEG Materials in Contact with Proteins. *ACS Appl. Mater. Interfaces* **2015**, *7*, 16881−16888.
(18) al-Ani, A.; Pingle, H.; Reynolds, N. P.; Wang, P.-Y.; Kingshott, P. Tuning the Density of Poly(ethylene glycol) Chains to Control Mammalian Cell and Bacterial Attachment. *Polymer* **2017**, *9*, 343.
(19) Carlmark, A.; Malmström, E. Atom Transfer Radical Polymerization from Cellulose Fibers at Ambient Temperature. *J. Am. Chem. Soc.* **2002**, *124*, 900−901.
(20) Matyjaszewski, K.; Dong, H.; Jakubowski, W.; Pietrasik, J.; Kusumo, A. Grafting from Surfaces for "Everyone:" ARGET ATRP in the Presence of Air. *Langmuir* **2007**, *23*, 4528−4531.
(21) Li, X.; Prukop, S. L.; Biswal, S. L.; Verduzco, R. Surface Properties of Bottlebrush Polymer Thin Films. *Macromolecules* **2012**, *45*, 7118−7127.
(22) Yan, W.; Fantin, M.; Ramakrishna, S.; Spencer, N. D.; Matyjaszewski, K.; Benetti, E. M. Growing Polymer Brushes from a Variety of Substrates under Ambient Conditions by Cu0-Mediated Surface-Initiated ATRP. *ACS Appl. Mater. Interfaces* **2019**, *11*, 27470−27477.
(23) Zhang, H.; Zhao, T.; Newland, B.; Liu, W.; Wang, W.; Wang, W. Catechol Functionalized Hyperbranched Polymers as Biomedical Materials. *Prog. Polym. Sci.* **2018**, *78*, 47−55.
(24) Gao, Q.; Li, P.; Zhao, H.; Chen, Y.; Jiang, L.; Ma, P. X. Methacrylate-ended Polypeptides and Polypeptoids for Antimicrobial and Antifouling Coatings. *Polym. Chem.* **2017**, *8*, 6386−6397.
(25) Morgese, G.; Verbraeken, B.; Ramakrishna, S. N.; Gombert, Y.; Cavalli, E.; Rosenboom, J. G.; Zenobi-Wong, M.; Spencer, N. D.; Hoogenboom, R.; Benetti, E. M. Chemical Design of Non-Ionic Polymer Brushes as Biointerfaces: Poly(2-oxazine)s Outperform Both Poly(2-oxazoline)s and PEG. *Angew. Chem., Int. Ed.* **2018**, *57*, 11667−11672.
(26) Barbey, R.; Lavanant, L.; Paripovic, D.; Schüwer, N.; Sugnaux, C.; Tugulu, S.; Klok, H.-A. Polymer Brushes via Surface-Initiated Controlled Radical Polymerization: Synthesis, Characterization, Properties, and Applications. *Chem. Rev.* **2009**, *109*, 5437−5527.
(27) Azzaroni, O. Polymer Brushes Here, There, and Everywhere: Recent Advances in Their Practical Applications and Emerging Opportunities in Multiple Research Fields. *J. Polym. Sci., Part A: Polym. Chem.* **2012**, *50*, 3225−3258.
(28) Divandari, M.; Trachsel, L.; Yan, W.; Rosenboom, J.-G.; Spencer, N. D.; Zenobi-Wong, M.; Morgese, G.; Ramakrishna, S. N.; Benetti, E. M. Surface Density Variation within Cyclic Polymer Brushes Reveals Topology Effects on Their Nanotribological and Biopassive Properties. *ACS Macro Lett.* **2018**, *7*, 1455−1460.
(29) Kang, T.; Banquy, X.; Heo, J.; Lim, C.; Lynd, N. A.; Lundberg, P.; Oh, D. X.; Lee, H.-K.; Hong, Y.-K.; Hwang, D. S.; Waite, J. H.; Israelachvili, J. N.; Hawker, C. J. Mussel-Inspired Anchoring of Polymer Loops That Provide Superior Surface Lubrication and Antifouling Properties. *ACS Nano* **2016**, *10*, 930−937.
(30) Shin, E.; Lim, C.; Kang, U. J.; Kim, M.; Park, J.; Kim, D.; Choi, W.; Hong, J.; Baig, C.; Lee, D. W.; Kim, B.-S. Mussel-Inspired Copolyether Loop with Superior Antifouling Behavior. *Macromolecules* **2020**, *53*, 3551−3562.
(31) Divandari, M.; Morgese, G.; Trachsel, L.; Romio, M.; Dehghani, E. S.; Rosenboom, J.-G.; Paradisi, C.; Zenobi-Wong, M.; Ramakrishna, S. N.; Benetti, E. M. Topology Effects on the Structural and Physicochemical Properties of Polymer Brushes. *Macromolecules* **2017**, *50*, 7760−7769.
(32) Yan, W.; Divandari, M.; Rosenboom, J.-G.; Ramakrishna, S. N.; Trachsel, L.; Spencer, N. D.; Morgese, G.; Benetti, E. M. Design and Characterization of Ultrastable, Biopassive and Lubricious Cyclic Poly(2-alkyl-2-oxazoline) Brushes. *Polym. Chem.* **2018**, *9*, 2580−2589.
(33) Yan, W.; Ramakrishna, S. N.; Romio, M.; Benetti, E. M. Bioinert and Lubricious Surfaces by Macromolecular Design. *Langmuir* **2019**, *35*, 13521−13535.
(34) Johnson, K. L.; Kendall, K.; Roberts, A. D. Surface Energy and the Contact of Elastic Solids. *Proc. R. Soc. Lond. A* **1971**, *324*, 301−313.
(35) Olsén, P.; Borke, T.; Odelius, K.; Albertsson, A.-C. ε-Decalactone: A Thermoresilient and Toughening Comonomer to Poly(l-lactide). *Biomacromolecules* **2013**, *14*, 2883−2890.
(36) Beckingham, B. S.; Sanoja, G. E.; Lynd, N. A. Simple and Accurate Determination of Reactivity Ratios Using a Nonterminal Model of Chain Copolymerization. *Macromolecules* **2015**, *48*, 6922−6930.
(37) Israelachvili, J.; Min, Y.; Akbulut, M.; Alig, A.; Carver, G.; Greene, W.; Kristiansen, K.; Meyer, E.; Pesika, N.; Rosenberg, K.;

https://doi.org/10.1021/acs.biomac.1c01124
Biomacromolecules 2021, 22, 5173−5184

Zeng, H. Recent Advances in the Surface Forces Apparatus (SFA) Technique. *Rep. Prog. Phys.* **2010**, *73*, No. 036601.
(38) Çaykara, T.; Sande, M. G.; Azoia, N.; Rodrigues, L. R.; Silva, C. J. Exploring the Potential of Polyethylene Terephthalate in the Design of Antibacterial Surfaces. *Med. Microbiol. Immunol.* **2020**, *209*, 363−372.

https://doi.org/10.1021/acs.biomac.1c01124
Biomacromolecules 2021, 22, 5173−5184